Magnetic structure of spin-density waves in Cr(001)/Sn multilayers with periodic monatomic spacer layers of nonmagnetic Sn

M. Takeda*
Physics Department, Graduate School of Science, Tohoku University, Sendai 980-8578, Japan

K. Mibu† and T. Shinjo‡
Institute for Chemical Research, Kyoto University, Uji 611-0011, Japan

Y. Endoh
Institute for Material Research, Tohoku University, Sendai 980-8577, Japan

J. Suzuki
Advanced Science Research Center, Japan Atomic Energy Research Institute (JAERI), Tokai, Ibaraki 319-1195, Japan
(Received 28 February 2004; published 15 September 2004)

Detailed magnetic structure of spin-density waves (SDWs) in epitaxial Cr(001)/Sn multilayers was investigated by neutron scattering combined with Mössbauer spectroscopic studies. Monatomic Sn layers were embedded in 240-nm-thick Cr(001) films with varying the periodic spacing from 4.2 to 16.2 nm. All samples were revealed to be a commensurate antiferromagnetic (CAF) phase at 300 K. The CAF structures changed to incommensurate SDW states with complex wave forms whose wavelength are controlled by the artificial periodicity at low temperatures although the CAF structure in the sample with the period of 4.2 nm persisted even at 10 K. The phase transition depends on the thickness of the Cr layers intervening between Sn monatomic layers. An appreciable phase slip in the SDW was observed during the phase transition in the sample with the period of 10.2 nm. The SDW structure is discussed by taking account of the competing forces between the nesting of Fermi surface and a pinning of antinodes at the Sn monatomic layers.

DOI: 10.1103/PhysRevB.70.104408 PACS number(s): 75.70.−i, 75.30.Fv, 75.25.+z, 76.80.+y

I. INTRODUCTION

Although it was recognized several decades ago that the spin-density wave (SDW) is realized in bulk Cr below the Néel temperature of 312 K in metallic Cr, the microscopic mechanism of the incommensurate SDW (ISDW) itself cannot be completely understood. In particular, the fact that the SDW state is sensitively changed by various environments such as the effect of impurity, internal stress, and external pressure has been the subject of the Fermi surface effect.[1] In addition, magnetic properties are drastically modified in thin films, and the magnetic properties of Cr in multilayers are very sensitive to the thickness of Cr layers and the counterpart elements of the bilayers.[2–7] These facts are still issues of the effect of the band structure near the interfaces in Cr multilayers itself or the magnetic interaction at the interface with counter magnetic elements. This subject is also related to the giant magnetoresistance effect of Fr/Cr multilayers, where the magnetic transport properties are strongly influenced by the structure of the multilayers and the proximity effect.[3–5]

One way to solve these issues is to study the SDW state in Cr/nonmagnetic metal multilayers. In this respect, we have been investigating Cr(001)/Sn multilayers in which monatomic Sn layers are periodically inserted in the Cr(001) epitaxial films and reported the existence of exotic SDW states in the multilayers.[8–12] In these multilayers, the ISDWs are stabilized at low temperatures. The structure is, however, not the same as that in bulk Cr but very exotic one. The most striking feature of the ISDWs is that their wavelength is not simply controlled by the nesting vector of the Fermi surface but by the artificial periodicity introduced by the embedded Sn monatomic layers. This suggests that the band nesting and the periodic potential by the Sn spacer layers in these multilayers are competing with each other. Nevertheless, the SDW state in Cr(001)/Sn epitaxial multilayers, where the SDW structure in bulk Cr is modified by the insertion of the nonmagnetic spacer, gives a direct evidence of the wave nature of the SDW in metallic Cr. We report here detailed results of neutron diffraction studies from the Cr(001)/Sn multilayers including the dependence on multilayer periodicity at various temperatures, which was not shown in the previous letter, and discuss the microscopic mechanism of the SDW stability in Cr.

II. EXPERIMENT

Stacked bilayers of $[\mathrm{Cr}(t_{\mathrm{Cr}})/\mathrm{Sn}(0.2\ \mathrm{nm})]$ (t_{Cr}=4.0, 8.0, 10.0, 12.0, and 16.0 nm) were epitaxially grown on MgO(001) substrates at 473 K with a 5-nm-thick Cr buffer layer with ultra-high vacuum deposition. The stacking number of the bilayer in each sample, M, was determined to make the accumulated thickness of Cr to be 240 nm ($t_{\mathrm{Cr}} \times M = 240$ nm). According to the thickness of each Cr layer separated by the monatomic Sn, t_{Cr} in a unit of nanometers, the samples are denoted as CS4, CS8, CS10, CS12, CS14, and CS16, respectively. A thin Cr layer with a thickness of 240 nm (C240) was also synthesized on the same

substrate and buffer in order to clarify the effect of inserting Sn spacer layers. Due to a well-established epitaxial conditions, the MgO[001] and the body-centered-cubic (bcc) Cr[001] directions are normal to the sample plane, and the MgO[110] and the Cr[010] are parallel to each other in the film plane. We define the Cr[001] direction in the reciprocal space as L and the [010] direction as K hereafter. Details of the sample preparation procedure have already been reported in Ref. 8.

Neutron diffraction measurements were performed on conventional triple-axis spectrometers, TOPAN, TAS-1, and TAS-2 at JRR-3M in JAERI. The incident neutron energy was fixed at 14.7 or 13.7 meV using a vertically focusing PG(002) monochromator, and the higher order contamination was removed by a PG filter before the samples. A vertically focusing PG(002) analyzer was used in order to detect only an elastic component. The horizontal collimations were chosen to be 100′-30′-30′-100′ for TOPAN and 100′-40′-40′-100′ for TAS-1 and TAS-2. The samples were mounted in Al cans filled with He gas, which were attached to the cold head of a refrigerator. The stability of temperature during the measurements was ±0.02 K.

Scans were performed along the L and K directions through the (001) and (010) reciprocal points of the bcc [body-centered-tetragonal (bct)] Cr films, where the nuclear peaks of the bcc (bct) structure are forbidden. In bulk Cr the spin reorientation occurs at 123 K from the transverse SDW (TSDW) to the longitudinal SDW (LSDW) with decreasing temperature. In thermal equilibrium the multiple $\boldsymbol{Q}$ state is realized, where the propagation vectors of SDW $\boldsymbol{Q}$ and the spin orientations are parallel to one of the bcc principal axes, and all their combinations coexist with equal probability. In the multiple $\boldsymbol{Q}$ state, the satellite peaks originating from the TSDW states appear at $(\pm\delta,0,1)$, $(0,\pm\delta,1)$, and $(0,0,1\pm\delta)$ around the (001) position in a neutron diffraction profile. The satellites are observed only at $(0,0,1\pm\delta)$ in the case of the single $\boldsymbol{Q}$ state where the $\boldsymbol{Q}$ is parallel to the L direction. The single $\boldsymbol{Q}$ state can be realized by the field cooling process across the Néel temperature with sufficient magnetic fields along the L direction. The incommensurability δ in bulk Cr is defined as $\delta=1-|\boldsymbol{Q}|$, where $\boldsymbol{Q}$ is measured in units of $2\pi/a$.[1] In the following sections we denote the scan along the L direction as L scan and that along the K direction as K scan. These scans are schematically displayed in Fig. 1.

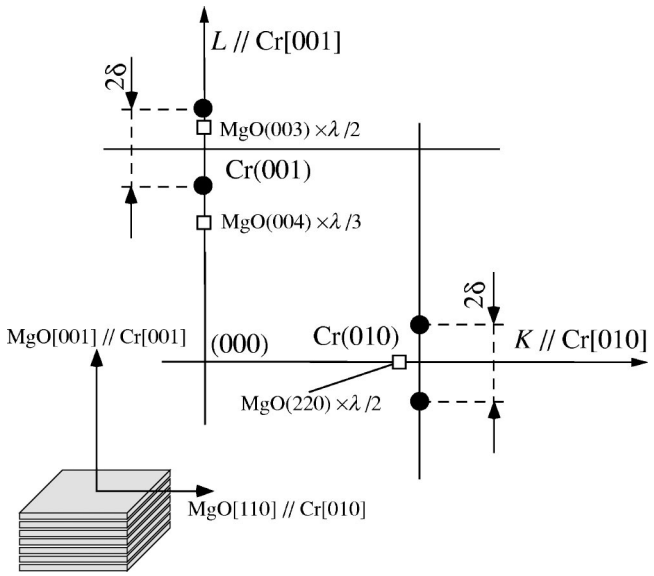

FIG. 1. Schematic representation of reciprocal plane for Cr(001)/Sn epitaxial films. Scans were performed along the principal axes through the (010) and (001) reciprocal points, where the nuclear reflections for bcc Cr are forbidden. Satellite peaks from incommensurate antiferromagnetic structures with the propagation vector parallel to the (001) direction would appear at $(0,0,1\pm\delta)$ and $(0,1,\pm\delta)$ in bulk Cr of the single Q state parallel to the L direction as indicated by solid circles. Several peaks from the MgO substrate (□) appear in the scans. The lower left shows the epitaxial relation between MgO and Cr in real space.

III. SAMPLE CHARACTERIZATION

The multilayer structure with the desired artificial periodicity was confirmed to be well established by observing well-defined satellite peaks around Cr(002) as many as the fourth order by conventional x-ray diffractometry. Figure 2 shows the $\Lambda(=t_{Cr}+t_{Sn})$ dependence of in-plane and out-of-plane lattice parameters measured by TAS-1 and TAS-2 at ambient temperature where all of the samples show a commensurate antiferromagnetic (CAF) structure.[10] The lattice parameters were determined from the peak positions of Cr(010) and Cr(001) because Cr(020) and (002) peaks could not be identified due to the large peak of Al(220) from the Al can. Some of the parameters in Fig. 2 were also deduced from the peak positions of Cr(020) and Cr(002) by the measurements with the samples outside the Al can. The values obtained by the conventional x-ray diffractometer are also shown. Both in-plane (010) and out-of-plane (001) lattice constants were expanded in comparison with bulk Cr. However, they gradually approach the bulk value with increasing Λ. The in-plane lattice constants were larger than the out-of-plane ones except CS10. Therefore, the crystal structure of these multilayers is not bcc but bct. Note that the obtained out-of-plane lattice constants are averaged ones of Cr-Cr and Cr-Sn. The Λ de-

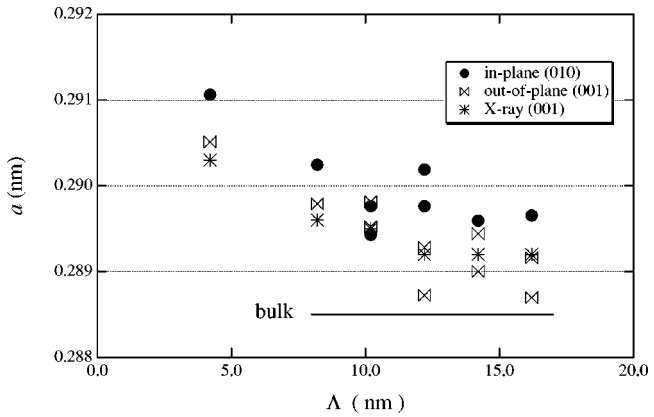

FIG. 2. The artificial period, Λ, dependence of in-plane (001) and out-of-plane (001) average lattice parameters of Cr/Sn(001) multilayers measured by neutron and x-ray diffractions.

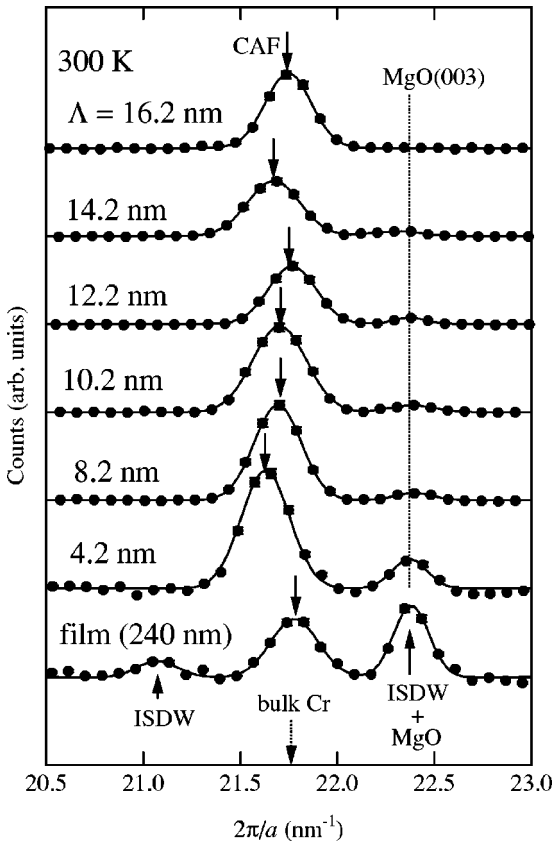

FIG. 3. Peak profiles by L scans of Cr/Sn multilayers and Cr thin film (240 nm) through (001) reciprocal point at 300 K. $\Lambda(=t_{Cr}+t_{Sn})$ indicates the artificial period of Cr/Sn multilayers. Solid lines are the fits to the data using Gaussians. Arrows indicate positions of Cr(001) which are equal to a half of those of Cr(002) peak. The existence of (001) peak shows a CAF structure of these samples. Peaks of the incommensurate spin-density wave are also observed in the thin film with thickness of 240 nm. Intensities of the forbidden peak of MgO(003) depend on quality of MgO substrates.

pendence and the anisotropy of lattice spacing leads to different internal stress in each sample.

Mössbauer spectra of these multilayers show sextets which correspond to the hyperfine fields between 9 and 11 T at ^{119}Sn nuclear positions at ambient temperature.[8] The hyperfine field distribution is quite different from that observed at ^{119}Sn dispersed in bulk Cr, where the hyperfine field continuously distributed between 0 and 12 T.[13] The hyperfine field does not change so much with decreasing temperature although the magnetic phase transition from the CAF and SDW state occurs between 300 and 20 K.[12] This large hyperfine field is consistent with the fact that the Neél temperature of these multilayers is much higher than that of bulk Cr, and that all of the multilayers have the CAF structure at 300 K, which was confirmed by the neutron diffraction measurements.[10]

Figure 3 shows neutron diffraction profiles at 300 K by L scans of the Cr/Sn multilayers and Cr thin film (C240) through the (001) position. The multilayer period is indicated by Λ. Intensities are normalized by the intensity of the Cr(002) nuclear peak except C240. The single peak appearing on the position at exactly a half of the reciprocal lattice position of (002) indicates the existence of the CAF structure at 300 K in all multilayers examined in this study.

The peak at 22.4 nm^{-1} in Fig. 3, which is remarkable in the profile of CS4 and C240, can be assigned to be (003) forbidden peak of MgO substrate exposed by $\lambda/2$ contaminated incident neutrons. As reported in Ref. 9, the CAF peak at 21.8 nm^{-1} in C240 at 300 K disappears at 20 K, while the peak of MgO(003) was still observed with almost the same intensity. The temperature dependent feature of the (001) peak shows that this peak does not arise from $\lambda/2$ contamination of the Cr(002) reflection but from the CAF structure. Intensities of (001) peak in the other multilayers also decreased with decreasing temperature as shown in the following section. To summarize, the CAF structure is formed in all multilayered samples and that an ISDW coexists in C240 at 300 K. The rather large $\lambda/2$ component from MgO(003) in the CS4 and C240 profile may be caused by the poor quality of MgO substrates.

The integrated intensities of the (001) and (010) are not equal even after normalized by (020) and (002) of bct Cr nuclear peaks. This difference indicates either a CAF with noncollinear structure in a single magnetic domain or the volume distribution of domains of CAFs with different spin polarization which is parallel to one of the principle axes of bct structure (multi-S domain). In the former case the intensity of (010) peak is proportional to the sum of squared in-plane [100] and out-of-plane [001] components of Cr spins, and that of (001) to the sum of two squared in-plane components of [100] and [010]. In the latter case, the (010) intensity represents the sum of the volume of in-plane [100] and out-of-plane [001] S domains of CAF, and the (001) intensity is proportional to that of two in-plane S domains of [100] and [010].

The averaged spin polarization deduced from the intensity ratios are [112], [223], [111], [112], [112], and [223] for CS4, CS8, CS10, CS12, CS14, and CS16 in this order. The direction of each sample is one of [111], [112], and [223]. However, there is no systematic correlation between Λ and the direction. It is known that the easy axes of the ISDW in bulk Cr are bcc principle axes. The hard axis of bulk Cr like [111] is unlikely to be the easy axes of these multilayers. Therefore, it is natural to conclude that the ratios indicate the volume fraction of multi-S domains. The Mössbauer studies, however, have revealed that an averaged spin polarization is always the same for samples with the same multilayer structure, although it is expected that the volume fraction of the S domains may vary under a slight difference in condition of synthesize.[14] At the moment we cannot determine experimentally which case is realized in these multilayers. Although some uncertainties are included, Table I shows the volume fraction of S domains for the multi-S domain model, and the magnitude and direction of averaged Cr spins. In comparison with the low-temperature value of bulk Cr, CS4 has almost the same magnitude of moment.

IV. DIFFRACTION PROFILES AT LOW TEMPERATURES

Neutron diffraction profiles of L scans across the (001) and (010) at 20 K are displayed in Figs. 4(a) and 4(b). The

TABLE I. The designed artificial period, Λ, the volume fraction of *S* (spin polarization) domains in the case of multi-*S* domain state, the averaged spin polarization, and the magnitude of Cr spins deduced from neutron diffraction measurements at 300 K. The averaged spin polarization corresponds to possible easy axes in the case that a single-*S* domain is realized in the sample.

	Multi-*S* domain			
Designed artificial period Λ(nm)	In-plane components (%)	Out-of-plane components (%)	Averaged spin polarization M(300 K)(μ_B)	
4.2	37	63	[112]	0.57±0.19
8.2	51	49	[223]	0.44±0.10
10.2	68	32	[111]	0.38±0.08
12.2	32	68	[112]	0.43±0.16
14.2	32	68	[112]	0.44±0.08
16.2	47	53	[223]	0.39±0.10

difference of half width at half maximum (HWHM) of the peaks in both figures arises from the resolution effect. It means that the resolution for the scans parallel to the scattering vector is broader than that of the perpendicular case. Nevertheless, the HWHM of each peak reaches the resolution limit. It was confirmed that a long-range incommensurate magnetic order of Cr along the *L* direction is formed across the Sn monatomic layers.

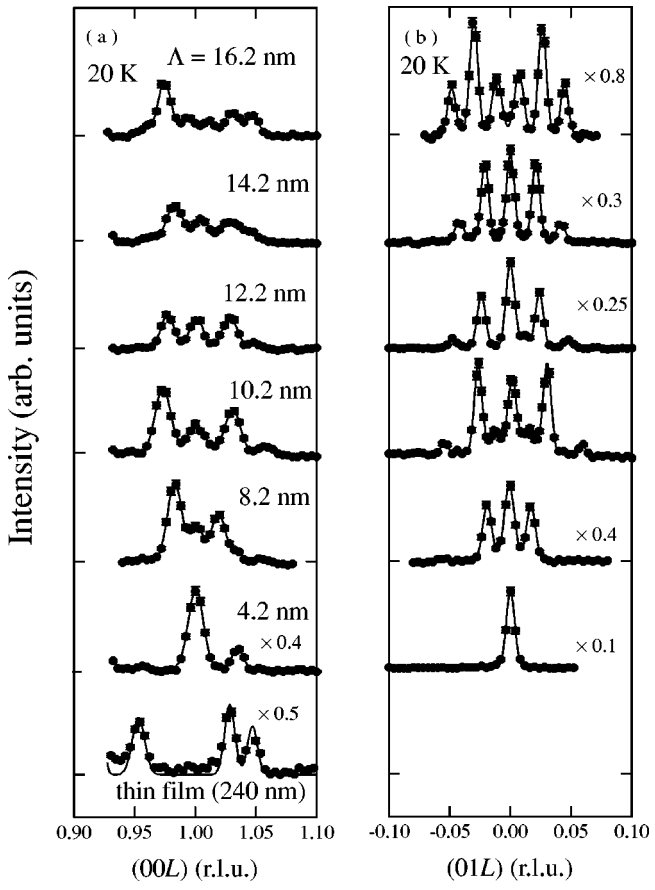

FIG. 4. *L* scans of Cr/Sn multilayers and Cr thin film (240 nm) through (a) (001) and (b) (010) reciprocal points at 20 K. Solid lines are the fits to the data using Gaussians. There is a large peak of MgO(002) at (00 0.92), which is removed in Fig. 4(a).

In these figures each scan is normalized by the same factor as used in the normalization of corresponding scan at 300 K. It is noted that the intensities are multiplied by different factors in order to show the peak height almost constant. The difference in intensities between Figs. 4(a) and 4(b) comes from the fact that the spin polarization or the volume ratio of *S* domains is dependent on the sample. However, the ratio of integrated intensities of *K* and *L* scans is almost constant between 300 and 20 K. Therefore, it seems that no spin reorientation like the transition from TSDW to LSDW in bulk Cr at 123 K occurs. Total integrated intensity at 20 K is slightly larger (20%) than that of CAF peak at 300 K in both *K* and *L* scans.

The CAF peak of C240 at 300 K was no longer detected at 20 K. The peak splits into two satellite peaks at 0.953 and 1.047 r.l.u. This shows that the SDW is formed in the *L* direction as observed in an epitaxial Cr(001) film of 300 nm thick on $Al_2O_3(1\bar{1}02)$ substrates.[15] From the δ=0.047 r.l.u. we find that the wavelength of the ISDW is equal to 6.2 nm in real space. The deviation of δ from the bulk value and the transition from the CAF structure to the ISDW are consistent with the phase diagram reported in Ref. 15.

The CAF structure persists in CS4 down to 20 K. The thickness of each Cr layer in CS4, 4.0 nm, is shorter than the wavelength of ISDW in bulk Cr. We speculate that the thickness of one Cr layer is not long enough to form ISDW in this sample. It is consistent with the other observation in either thin Cr films or other multilayered and trilayered systems.[3–7,16] A tiny peak emerges in the *L* scan at (00 0.96). The magnitude of δ is equal to that of C240. However, there is no corresponding peak at (00 1.04) nor in the *L* scan through (010). The origin of this peak is unclear.

For the other multilayers in which the artificial period, Λ, is longer than the nesting vector of bulk Cr, several satellite peaks appeared around (001) and (010) positions when the samples were cooled down to 20 K. No such satellite peaks were detected by the *K* scans through neither (001) nor (010) points. This indicates that all ISDWs are in the single $\boldsymbol{Q}$ state where the $\boldsymbol{Q}$ is parallel to out-of-plane, [001]. Because of no evidence of spin reorientation, the averaged spin polarization in each sample is the same as that listed in Table I. When a sample is in a single domain state, ISDW with canted spin

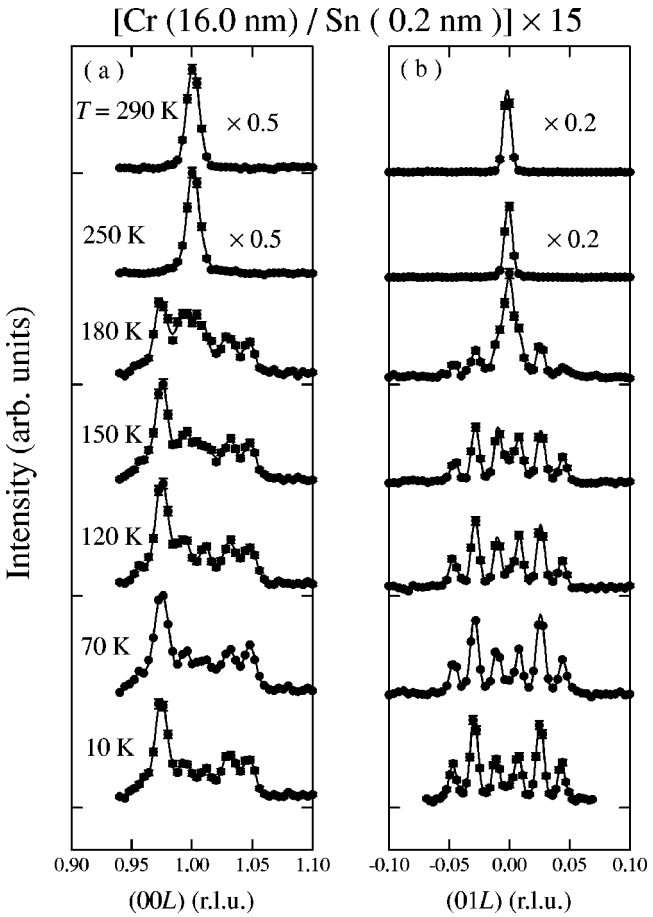

FIG. 5. The temperature dependence of (a) the (00L) and (b) (01L) scan profiles of Cr/Sn multilayer with artificial period of 16.2 nm.

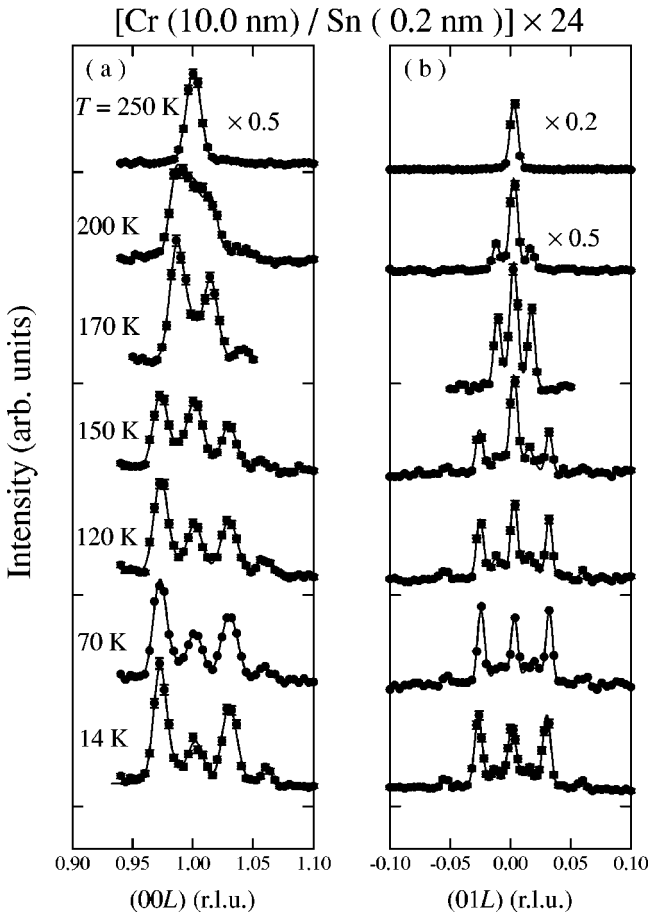

FIG. 6. The temperature dependence of (a) the (00L) and (b) (01L) scan profiles of Cr/Sn multilayer with artificial period of 10.2 nm.

from the bct crystallographic axes is realized in the sample. In the case of the multi-S domain state, TSDW and ISDW coexist with the volume fraction given in Table I.

The satellite peaks appear as several pairs at both sides of the CAF peak position. While the intensities of two satellites in each pair are almost identical in Fig. 4(b), apparent unbalance in intensities can be noted in Fig. 4(a). The similar asymmetry in intensities of satellite peaks originating in ISDW was observed in bulk Cr. It was revealed that the asymmetry indicated the existence of strain wave, and that degree of the unbalance depended on scalar product of a scattering vector and an amplitude vector of the stain wave.[17,18] Therefore, the present result indicates the existence of the strain wave in these multilayers with the amplitude vector along the perpendicular direction of the films. It is consistent with the difference of the in-plane and out-of-plane lattice parameter as shown in Fig. 2.

Figures 5 and 6 show the temperature dependence of L scan profiles of CS16 and CS10, respectively. The corresponding peak positions and integrated intensities are plotted in Figs. 7 and 8. At low temperatures the CAF peak at 300 K of CS16 gradually splits into sextet with keeping the total integrated intensity almost constant. In this sample the peak position of the satellite peaks little changes with changing temperature. In contrast, the CAF peak of CS10 also changes into multiplets at low temperatures, but the main satellite peaks, whose intensities are most dominant, abruptly changes between 170 and 150 K.

V. EXOTIC SPIN-DENSITY WAVES IN Cr/Sn MULTILAYERS

As reported in Refs. 9–12 combination of neutron scattering and ^{119}Sn Mössbauer spectroscopic studies made it clear that the satellite peaks in Fig. 4 are assigned to the fundamental and the higher harmonics of the ISDW whose wavelength is not simply governed by the nesting vector of the Fermi surface but dominantly by the multilayer period. The Mössbauer spectra indicated that the Cr spins adjacent to the Sn layers are enhanced and ferromagnetically coupled across the Sn monatomic layers. The enhancement is believed to cause a pinning of the Cr moments at Cr/Sn interfaces, and the pinning is likely to make antinodes of the ISDW at the interfaces.[12]

This exotic ISDW is composed of several higher harmonic components. It is convenient for indicating positions of the satellite peaks to introduce a new parameter, $\Delta = a_{001}/(2\Lambda)$, using the multilayer period and the lattice parameter of epitaxial Cr. By the new parameter, Δ, the posi-

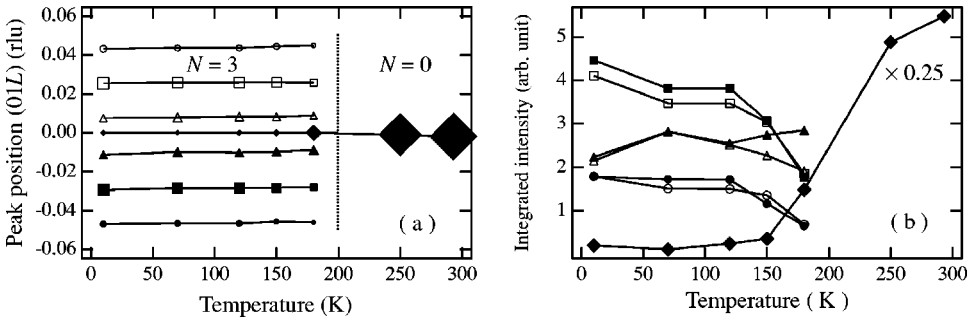

FIG. 7. The temperature dependence of (a) peak position and (b) integrated intensity of each satellite of Cr/Sn multilayer with artificial period of 16.2 nm in Fig. 5(b). Each symbol in (a) and (b) corresponds to the same satellite peak, and the size of symbols in (a) is proportional to integrated intensities of the corresponding peaks. A commensurate antiferromagnetic structure ($N=0$) at 300 K changes into an ISDW with three nodes ($N=3$) in the Cr layers at low temperatures without undergoing an ISDW with $N=1$.

tions of all peaks can be assigned as $(0,1,\pm N\Delta)$ and $(0,0,1\pm N\Delta)$ where N is a positive integer. For example in CS8 two pairs of satellite peaks appeared at $(0,1,\pm\Delta)$ and $(0,0,1\pm\Delta)$.[10]

From the positions of satellites, the period or wavelength, λ, of each modulation of magnetic structure in real space can be obtained. The λ vs Λ is plotted by solid circles in Fig. 9. The size of each circle is proportional to the averaged integrated intensities of $(0,1,\pm N\Delta)$ in the L scans through (010) for each sample. The integrated intensities of peak at the CAF position are also plotted as $\lambda=\infty$. This figure shows that all the circles are located on one of the lines

$$\lambda = \Lambda/N, \quad N = 1,\ 2,\ 3,\ 4,\ 5,\ \text{and}\ 6. \tag{1}$$

This clearly indicates that the λ is defined by the artificial period, Λ.

Once we know that the antinodes of sinusoidal waves are located at Cr/Sn interfaces, it is ready to notice that N corresponds to the number of nodes in each Cr layer intervening between Sn monatomic layers. The N also represents a symmetry of sinusoidal waves of each harmonics. Even (odd) functional sinusoidal waves therefore give rise to the even (odd) satellites. Furthermore, these higher harmonics couple only with those of the same symmetry (even or odd). For examples, in CS8 only the first and the third harmonics couple with each other, whereas the CAF peak with $N=0$ is independent of the other harmonics with the odd N. It means that the ISDW and the CAF coexist at low temperatures in CS8. In the case of CS10 and CS14 all harmonics have even N. Therefore, all these harmonics may essentially couple and form highly distorted sinusoidal ISDW.

Model calculations of ^{119}Sn Mössbauer spectra for the ISDW with the higher harmonics showed that the spectra were very sensitive to the sign and amplitude of the harmonics.[19,20] Actually the existence of the highly distorted ISDW has been revealed in polycrystals of Cr and Cr alloys[13] and in the vicinity of surface region of bulk single-crystal Cr[21] by the single use of ^{119}Sn Mössbauer spectroscopy. In the present study we will show concrete wave forms of the ISDW in Cr/Sn multilayers deduced from the neutron diffraction profiles. However, the results of Mössbauer spectroscopic studies are also very important for the reconstruction as described later. Without the information given by the Mössbauer spectroscopy we could not determine the position of nodes or antinodes of the ISDW.

When the spins $\boldsymbol{S}_{\boldsymbol{l}}$ of site $\boldsymbol{l}$ is described by

$$\boldsymbol{S}(\boldsymbol{l}) = \sum_{n=-\infty}^{+\infty} \boldsymbol{S}_{n\boldsymbol{Q}} \exp(in\boldsymbol{Q}\cdot\boldsymbol{l}), \tag{2}$$

the elastic magnetic neutron cross section can be written in the following equation:

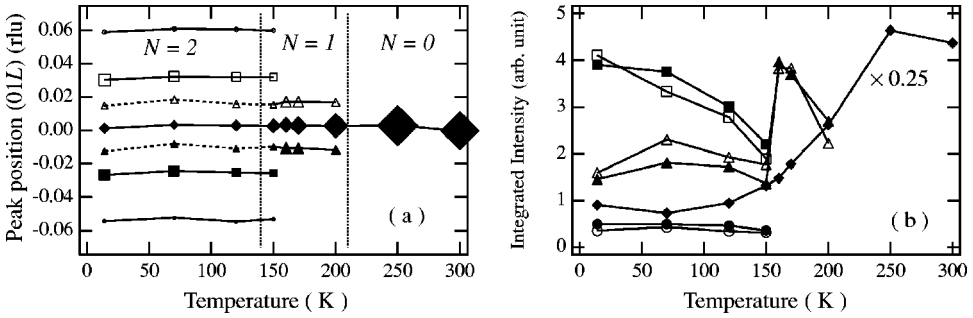

FIG. 8. The temperature dependence of (a) peak position and (b) integrated intensity of each satellite of Cr/Sn multilayer with artificial period of 10.2 nm in Fig. 6(b). Each symbol in (a) and (b) corresponds to the same satellite peak, and the size of symbols in (a) is proportional to integrated intensities of the corresponding peaks. Two transitions of the number of the nodes, N, from 2 to 1 and from 1 to 0 occur between 10 and 290 K.

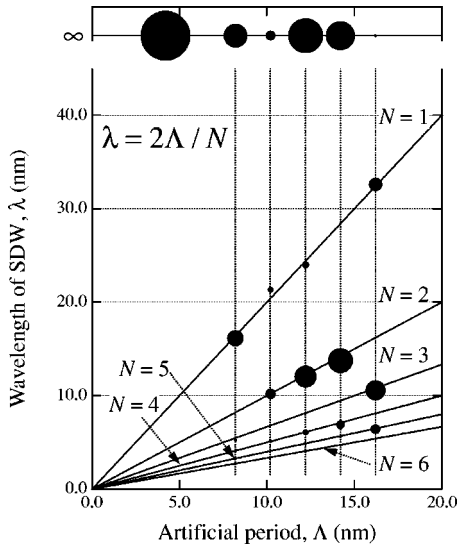

FIG. 9. Relation between the period of modulation of the SDW, λ, and the multilayer period, Λ. The modulation periods were obtained from the position of the satellite peaks in Fig. 4(b). Solid linear lines are $\lambda=\Lambda/N$ ($N=1$, 2, 3, 4, 5, and 6). The commensurate antiferromagnetic SDW (CAF) corresponds to $N=0$ and $\lambda=\infty$. The size of each circle is proportional to the intensity of the corresponding diffraction peak.

$$\frac{d\sigma}{d\Omega} \propto \sum_{\boldsymbol{\tau}} \sum_{n=-\infty}^{\infty} |f_m(\boldsymbol{\tau})|^2 \delta(\boldsymbol{\kappa}+n\boldsymbol{Q}+\boldsymbol{w}-\boldsymbol{\tau}) \times(|\mathbf{S}_{n\boldsymbol{Q}}|^2-|\boldsymbol{S}_{n\boldsymbol{Q}}\cdot\hat{\boldsymbol{\kappa}}|^2) \quad (n=0,\pm1,\pm2,\ldots,\pm\infty). \tag{3}$$

Here $\boldsymbol{\kappa}$ is the scattering vector, $\hat{\boldsymbol{\kappa}}$ the unit vector of $\boldsymbol{\kappa}$, and $\boldsymbol{\tau}$ the reciprocal vector of bct structure

$$\boldsymbol{\tau}=\frac{2\pi}{a}\left(h,k,\frac{a}{c}l\right) \quad (h+k+l=\text{even integer}), \tag{4}$$

$f_m(\boldsymbol{\tau})$ the magnetic form factor, and the reciprocal vector $\boldsymbol{w}$ is defined by

$$\boldsymbol{w}=\frac{2\pi}{a}\left(1,1,\frac{a}{c}\right) \tag{5}$$

describing two sites in the bct unit cell; i.e., $\exp(i\boldsymbol{w}\cdot\boldsymbol{l})=+1$ for the corner atoms and $\exp(i\boldsymbol{w}\cdot\boldsymbol{l})=-1$ for the body centered atoms. Here a is the in-plane lattice constant, and c the out-of-plane one.

Although neutron scattering experiments give no information on a phase of each component of the higher harmonics in Eq. (2), we can reproduce the wave form of the ISDW under following simple assumptions; (1) all of the harmonics have antinodes (or nodes) at the interfaces, (2) all harmonics with the same symmetry, the even n or the odd n, are coupled, and (3) the directions of spin polarization of all the harmonics which form a single ISDW are common.

In the present multilayers the propagation vector of ISDW is parallel to L direction. If the ISDW is TSDW and spin polarization of all the harmonics is parallel to x (// [100]) direction, the integrated intensities of each satellite around $\boldsymbol{\tau}-\boldsymbol{w}=(001)$ and (010) in Fig. 4 becomes

$$I_n(\boldsymbol{\kappa}) \propto f_n^2 \delta(\boldsymbol{\kappa}+n\boldsymbol{Q}+\boldsymbol{w}-\boldsymbol{\tau}), \tag{6}$$

$$f_n = \pm|S^x_{n\boldsymbol{Q}}| \quad (n=0,\pm1,\pm2,\ldots,\pm\infty), \tag{7}$$

and the spins at the site $\boldsymbol{l}$ can be written as

$$S_x(\boldsymbol{l}) = f_0 + 2\sum_k^{+\infty} f_{2k}\cos(2k\boldsymbol{Q}\cdot\boldsymbol{l}), \tag{8}$$

or

$$S_x(\boldsymbol{l}) = 2\sum_k^{+\infty} f_{2k-1}\cos\{(2k-1)\boldsymbol{Q}\cdot\boldsymbol{l}\}, \tag{9}$$

with $k=1,2,\ldots,+\infty$. Equation (6) indicates that the higher harmonics with $n\boldsymbol{Q}$ appears as the satellite at $(0,1,n|\boldsymbol{Q}|)$ or $(0,0,1-n|\boldsymbol{Q}|)$. Therefore, the relation between Δ and $\boldsymbol{Q}$ is

$$N\Delta = |n\boldsymbol{Q}|. \tag{10}$$

Note that Eq. (3) is too simple because the asymmetry in intensity of the $\pm N$ satellites cannot be explained, which was observed in the L scans around (001) in Fig. 4(a). As already mentioned the asymmetry in intensity stems from the strain wave whose amplitude vector is parallel to the L direction. For the sake of simplicity, the asymmetry was not taken into account in the calculation and analysis. However, the profile around (010) in Fig. 4(b) can be safe for quantitative analysis by using this equation.

The sign of each coefficient of Eq. (7) cannot be determined even by the earlier mentioned hypothesis. Four combinations of the signs ($|f_0|\pm|f_2|\pm|f_4|$ or $|f_1|\pm|f_3|\pm|f_5|$) are possible for the first three terms. Since Mössbauer spectroscopic study suggested that the spins at interfaces are enhanced, two solutions to give reduced moments at the interface should be excluded.[11,12] Figure 10 shows the superimposed ISDWs in the real space, which composed of up to three harmonics with the combination of signs, (a) $|f_0|+|f_2|+|f_4|$ or $|f_1|+|f_3|+|f_5|$ and (b) $|f_0|+|f_2|-|f_4|$ or $|f_1|+|f_3|-|f_5|$. $|f_n|$s were obtained from the squared root of the integrated intensities of each satellite peak in Fig. 4(b). The wave forms corresponding to the TSDW with the propagation vector parallel to [001] are shown representatively. The solid lines corresponds to spins at the conners and the broken lines to those at the center of the bct unit cell. The dotted lines indicate the magnitude of spins if all the satellites gather to (010) position and make a fictitious single peak corresponding a CAF structure.

In bulk Cr the sign of f_3/f_1 in Eq. (9) was determined to be negative using intensity ratios of $I(1-\delta)/I(1+\delta)$ and

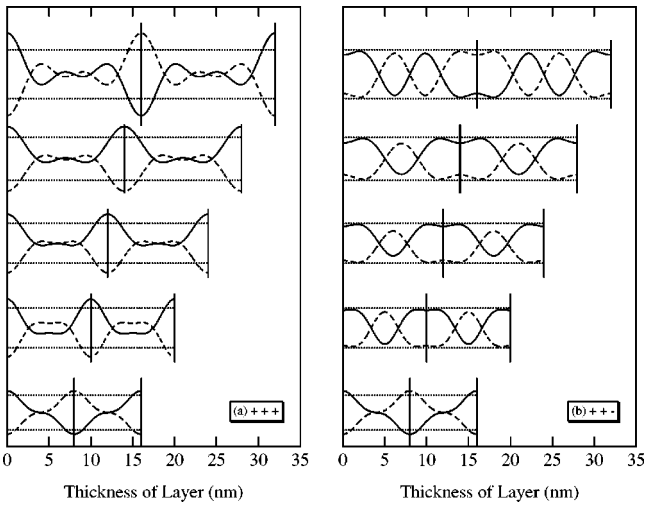

FIG. 10. Wave forms of the ISDW in real space reconstructed by the squared root of integrated intensity of satellite peaks shown in Fig. 4(b) using Eqs. (8) and (9). The solid lines correspond to spins at the conners and the broken lines to that at the center of the bct unit cell. The dotted lines indicate the magnitude of the spins in a fictitious CAF structure (see in text). Only waves with the same symmetry, odd or even, are coupled with each other. The three components are summed up (f_0, f_2, f_4 or f_1, f_3, f_5). Two of four possible combinations of the sign, (a) $|f_0|+|f_2|+|f_4|$ or $|f_1|+|f_3|+|f_5|$ and (b) $|f_0|+|f_2|-|f_4|$ or $|f_1|+|f_3|-|f_5|$, are displayed in these figures because the other two combinations give reduction of spins at the interfaces. An enhancement of spins at the interfaces is suggested by the Mössbauer spectroscopic study.

$I(1-3\delta)/I(1+3\delta)$.[17,18] Here $I(1\pm\delta)$ and $I(1\pm3\delta)$ are intensities of the fundamental and third harmonic satellites at $(1\pm\delta,0,0)$ and $(1\pm3\delta,0,0)$, respectively. This analysis may be also valid in these multilayers. It is, however, more complicated because it is necessary for the phase determination to analyze all the observable ratios of $I(1-nQ)/I(1+nQ)$.

In Fig. 10 it is assumed that the component with $N=0$ is superimposed with the other even components. In several cases in Fig. 10(a), this superimposition makes the resultant waves not to have clear nodes, which is defined as the zero-crossing point of the waves. On the other hands, the CAF, which is independent of the odd components, is thought to coexist with the ISDW for instance in CS8. The same coexistence cannot be excluded in the samples with ISDW composed of even harmonics. In this case the wave forms of the ISDW in CS10, CS12, and CS14 displayed in Fig. 10 are modified so that the solid and broken lines come together towards the 0 line and that clear nodes will appear.

First-principles electronic structure calculations of Fe/Cr multilayers have been done for the system with ideally flat interfaces and found that the Λ governs the wavelength of the ISDW instead of the nesting vector of Fermi surface.[22,23] It was independently predicted that the magnetic moments of Cr are enhanced at the interface of Cr/vacuum.[24] In the present case, instead of the proximity effect from the ferromagnetic layer the monatomic Sn layers are thought to have the same function as the vacuum for 3*d* electrons of Cr. In the present Cr/Sn multilayers the enhanced moments cause the pinning of the antinode of the ISDW at the interface although there is no proximity effect from Sn to Cr. This causes the similar situation between the Fe/Cr and Cr/Sn multilayers concerning the ISDW formation. The positions of satellite peaks of CS16 are insensitive to temperature as shown in Fig. 7. This rigidity of the peak positions were also observed in CS12.[10] This fact supports the idea that the wavelength of ISDW in these multilayers is governed not by the nesting of Fermi surface but by the artificial period, Λ.

On the contrary to CS12 and CS16, the peak positions of satellite peaks of CS10 abruptly change between 170 and 150 K. Below 200 K the satellites assigned to be $N=\pm1$ are clearly observed in the profiles in Figs. 6(a) and 6(b). However, intensities of these satellite decrease with further decreasing temperature. Instead of the satellites of $N=\pm1$, the other even components ($N=\pm2$ and ±4) become dominant below 150 K. It is very important that the phase transition of the number of nodes from $N=1$ to 2 followed by the transition from the CAF to the ISDW state was observed. Recently a similar temperature dependence has been reported for CrMn/Cr multilayers.[25]

This phase transition was theoretically predicted in Fe/Cr multilayers and trilayers by Shi *et al.*[26,27] In Ref. 27 it was reported that the number of nodes in Cr layers changes with temperature, and that the phase transition is strongly dependent on the energy mismatch between the electron and hole Fermi surface, and also on the interfacial roughness between Fe and Cr layers. Furthermore, the roughness also affects the location of the nodes and antinodes from the interfaces. In the present study we observed the phase transition from the CAF to the ISDW in all samples, while the phase transition to the different N only in CS10. According to the Λ-T diagram of Fig. 3 in Ref. 27, the distance of the phase boundaries between N and $N+1$ is closer in larger Λ. For the phase slip in CS12, CS14, and CS16 insufficient data points prevented the detailed investigations. If the nodes of the ISDW precisely lie at each interface, lack of the phase slip is predicted in Fe/Cr multilayers (model II in Ref. 27). For all the samples with t_{Cr} of 8 nm and larger in the present study it has been revealed that the antinodes are located at the interfaces. Therefore, model II may be excluded if the model is applicable similarly to Cr/Sn multilayers, although the magnetic function of Fe and Sn to the Cr at the interface differ with each other.

VI. CONCLUSIONS

We have investigated the magnetic structure of epitaxial Cr/Sn multilayers with periodically embedded monatomic Sn layers by complementary use of both neutron diffraction and ^{119}Sn Mössbauer spectroscopic measurements. The artificial period, Λ, is varied from 4.2 to 16.2 nm. The sample with $\Lambda=4.2$ nm has a CAF structure at 300 K, which persists down to 20 K. The samples with the larger Λ than 8.2 nm also have the CAF structures at 300 K. However, the phase transition from the CAF to ISDW occurs on cooling. The

wavelength of the ISDW is governed by Λ as a result of competition between the nesting vector of the Fermi surface and the artificial period. The additional phase transition between different number of the node in the ISDW state was observed in the sample of $\Lambda = 10.2$ nm. This phase slip is the direct evidence of competition between the temperature dependent nesting vector of Fermi surface and the rigid periodic potential introduced by multilayer period.

ACKNOWLEDGMENTS

The authors would like to express thanks for valuable technical assistance of M. Onodera and K. Nemoto in Tohoku University and Y. Shimojo in JAERI. This work was supported by Grants-in-Aid for Scientific Research and COE Research "Elements Science" (K.M. and T.S.) from the Ministry of Education, Science, Sports and Culture, Japan.

*Present address: Advanced Science Research Center, Japan Atomic Energy Research Institute (JAERI), Tokai, Ibaraki 319-1195, Japan. Electronic address: takeda@neutrons.tokai.jaeri.go.jp

†Present address: Research Center for Low Temperature and Materials Sciences, Kyoto University, Uji, Kyoto 611-0011, Japan.

‡Present address: International Institute for Advanced Studies, Kizugawadai, Kizu-cho, Kyoto 619-0225, Japan.

[1] E. Fawcett, Rev. Mod. Phys. **60**, 209 (1988).
[2] H. Zabel, J. Phys.: Condens. Matter **11**, 9303 (1999).
[3] E. E. Fullerton, S. D. Bader, and J. L. Robertson, Phys. Rev. Lett. **77**, 1382 (1996).
[4] A. Schreyer, C. F. Majkrzak, T. Zeidler, T. Schmitte, P. Bodeker, K. Theis-Bröhl, A. Abromeit, J. A. Dura, and T. Watanabe, Phys. Rev. Lett. **79**, 4914 (1997).
[5] A. Schreyer, J. F. Ankner, T. Zeidler, H. Zabel, M. Schäfer, J. A. Wolf, P. Grünberg, and C. F. Majkrzak, Phys. Rev. B **52**, 16 066 (1995).
[6] H. Fritzsche, S. Bonn, J. Hauschild, J. Klenke, K. Prokes, and G. J. McIntyre, Phys. Rev. B **65**, 144408 (2002).
[7] S. Demuynck, J. Meersschaut, J. Dekoster, B. Swinnen, R. Moons, A. Vantomme, S. Cottenier, and M. Rots, Phys. Rev. Lett. **81**, 2562 (1998).
[8] K. Mibu, S. Tanaka, and T. Shinjo, J. Phys. Soc. Jpn. **67**, 2633 (1998).
[9] M. Takeda, K. Mibu, K. Takanashi, K. Himi, Y. Endoh, T. Shinjo, and H. Fujimori, J. Phys. Soc. Jpn. **69**, 1590 (2000).
[10] M. Takeda, K. Mibu, T. Shinjo, J. Suzuki, and Y. Endoh, Appl. Phys. A: Mater. Sci. Process. **74**, s1554 (2002).
[11] K. Mibu and T. Shinjo, J. Phys. D **35**, 2359 (2002).
[12] K. Mibu, M. Takeda, J. Suzuki, A. Nakanishi, T. Kobayashi, Y. Endoh, and T. Shinjo, Phys. Rev. Lett. **89**, 287202 (2002).
[13] S. M. Dubiel, J. Magn. Magn. Mater. **124**, 31 (1993).
[14] K. Mibu and T. Shinjo (unpublished).
[15] P. Sonntag, P. Bödeker, A. Schreyer, and H. Zabel, J. Magn. Magn. Mater. **183**, 5 (1998).
[16] J. Unguris, R. J. Celotta, and D. T. Pierce, Phys. Rev. Lett. **69**, 1125 (1992).
[17] Y. Tsunoda, Y. Nakai, and N. Kunitomi, Solid State Commun. **16**, 443 (1975).
[18] S. Iida, Y. Tsunoda, Y. Nakai, and N. Kunitomi, J. Phys. Soc. Jpn. **50**, 2587 (1981).
[19] J. Cieślak and S. M. Dubiel, Nucl. Instrum. Methods Phys. Res. B **95**, 131 (1995).
[20] S. M. Dubiel, Recent Res. Devel. Physics **4**, 835 (2003).
[21] J. Cieślak and S. M. Dubiel, Phys. Status Solidi A **196**, 181 (2003).
[22] K. Hirai, Phys. Rev. B **59**, R6612 (1999).
[23] A. M. N. Niklasson, B. Johansson, and L. Nordström, Phys. Rev. Lett. **82**, 4544 (1999).
[24] G. Allan, Phys. Rev. B **19**, 4774 (1979).
[25] E. E. Fullerton, J. L. Robertson, A. R. E. Prinsloo, H. L. Alberts, and S. D. Bader, Phys. Rev. Lett. **91**, 237201 (2003).
[26] Z. P. Shi and R. S. Fishman, Phys. Rev. Lett. **78**, 1351 (1997).
[27] R. S. Fishman and Z. P. Shi, Phys. Rev. B **59**, 13 849 (1999).